Available online at www.sciencedirect.com
ScienceDirect
Journal of Magnetic Resonance 190 (2008) 233–247
JMR Journal of Magnetic Resonance
www.elsevier.com/locate/jmr

5- and 6-pulse electron spin echo envelope modulation (ESEEM) of multi-nuclear spin systems

B. Kasumaj *, S. Stoll [1]

ETH Zurich, Laboratory of Physical Chemistry, 8093 Zurich, Switzerland

Received 24 August 2007; revised 23 October 2007
Available online 6 November 2007

Abstract

In 3-pulse ESEEM and the original 4-pulse HYSCORE, nuclei with large modulation depth ($k \approx 1$) suppress spectral peaks from nuclei with weak modulations ($k \approx 0$). This cross suppression can impede the detection of the latter nuclei, which are often the ones of interest. We show that two extended pulse sequences, 5-pulse ESEEM and 6-pulse HYSCORE, can be used as experimental alternatives that suffer less strongly from the cross suppression and allow to recover signals of $k \approx 0$ nuclei in the presence of $k \approx 1$ nuclei. In the extended sequences, modulations from $k \approx 0$ nuclei are strongly enhanced. In addition, multi-quantum transitions are absent which simplifies the spectra. General analytical expressions for the modulation signals in these sequences are derived and discussed. Numerical simulations and experimental spectra that demonstrate the higher sensitivity of the extended pulse sequences are presented.

Keywords: Pulse EPR; ESEEM; HYSCORE; Cross-suppression effect; Multi-nuclear spin system; Phase cycling

1. Introduction

Pulse electron paramagnetic resonance (EPR) techniques in general and electron spin echo envelope modulation (ESEEM) techniques in particular are widely used to determine the electronic and geometric structure of paramagnetic species [1]. The results lead to unique insights into the electronic and geometric structure of paramagnetic centers in biological systems [2,3], as they allow for the determination of small hyperfine and quadrupole couplings of nuclear spins in the molecular environment of unpaired electrons.

Recent studies found that a cross-suppression effect [4,5] distorts signal intensities in standard ESEEM experiments (3-pulse ESEEM and 4-pulse HYSCORE) if more than one nucleus contribute to the signal and can thus lead to misinterpretation of ESEEM spectra. If all nuclei have a small modulation depth parameter k, i.e. a hyperfine interaction with a small anisotropic component and a small quadrupole coupling, this effect is negligible, the nuclei do not affect each other, and the spectrum equals the superposition of the single-nucleus spectra. On the other hand, the cross-suppression effect can have a strong impact in the presence of strongly modulating nuclei, as they can cause partial or complete suppression of signals from weakly modulating nuclei coupled to the same electron spin. In some circumstances, this results in spectra where weakly coupled nuclei cannot be observed at all, although they have a sufficiently large hyperfine coupling to be resolved. As these nuclei are often of structural or functional interest, experimental ways to circumvent or alleviate the impact of the cross suppression are desirable.

In this work, we examine two extended ESEEM pulse sequences, 5-pulse ESEEM [6] and 6-pulse HYSCORE [7], that can recover signals from weakly modulating nuclei and yield spectra that are less affected by cross suppression. These sequences give ESEEM spectra with peaks at the same positions as in 3-pulse ESEEM [8] and standard 4-pulse HYSCORE [9], respectively.

* Corresponding author. Fax: +41 44 632 1021.
E-mail address: besnik.kasumaj@phys.chem.ethz.ch (B. Kasumaj).
[1] Present address: Department of Chemistry, University of California, One Shields Ave, Davis, CA 95616, USA.

1090-7807/$ - see front matter © 2007 Elsevier Inc. All rights reserved.
doi:10.1016/j.jmr.2007.11.001

There are two reasons why spectra obtained with these extended sequences are less affected by cross suppression than the standard sequences. First, as we will show, they give substantially enhanced peak intensities for weakly modulating nuclei (those affected by cross suppression) and show decreased sensitivity towards strongly modulating nuclei (which are responsible for the cross suppression). The second reason is based on the occurence of blind spots [10,11]: In 3-pulse ESEEM and standard HYSCORE, a fixed inter-pulse delay of τ causes selective suppression of peaks at some frequencies, called blind spots. The cross-suppression effect can be counteracted by choosing τ so that peaks from strongly modulating nuclei that cause cross suppression fall on blind spots. The two extended pulse sequences have two experimentally adjustable fixed delays, τ_1 and τ_2, and they thus offer more flexibility in choosing blind spots.

This article is structured as follows: The theoretical background needed to derive and discuss the analytical expressions for the two extended sequences is summarized in Section 2. Section 3 gives details of the system and experiments used to illustrate our findings. The main part of the article is contained in Sections 5 and 6, where echo modulation signals for 2-, 3- and 5-pulse ESEEM and 4- and 6-pulse HYSCORE are compared theoretically and illustrated experimentally. Finally, Section 6 summarizes the insight obtained.

2. Theoretical background

The rotating-frame spin Hamiltonian, in angular frequency units, of an electron spin ($S=\frac{1}{2}$) coupled to N_I nuclei ($I_1=\cdots=I_{N_I}=\frac{1}{2}$) using the high-field approximation is given by [1,12]

$$H_0=\Omega_S S_z+\sum_{q=1}^{N_I}(\omega_{I,q}I_{z,q}+A_qS_zI_{z,q}+B_qS_zI_{x,q}), \tag{1}$$

where $\Omega_S=\omega_S-\omega_{\mathrm{mw}}$ is the offset between the electron resonance frequency ω_S and the frequency of the applied microwave (mw) pulse, ω_{mw}. $\omega_{I,q}=-g_{\mathrm{n},q}\mu_{\mathrm{n}}B_0/\hbar$ denotes the Larmor frequency of nucleus q.

In general, the hyperfine part of the Hamiltonian is related to the principal values $A_{11,q}$, $A_{22,q}$ and $A_{33,q}$ of the orthorhombic hyperfine interaction matrix $\boldsymbol{A_q}$, and two polar angles θ_q and ϕ_q describing the orientation of the external magnetic field $\boldsymbol{B}_0=(0,0,B_0)$ with respect to the frame where the hyperfine interaction matrix is diagonal [13]:

$$\begin{aligned}
A_q&=A_{33,q}\cos^2\theta_q+\sin^2\theta_q(A_{11,q}\cos^2\phi_q+A_{22,q}\sin^2\phi_q),\\
B_q&=\sqrt{B_{x,q}^2+B_{y,q}^2},\\
B_{x,q}&=\frac{1}{2}\sin\theta_q\cos\theta_q[(2A_{33,q}-A_{11,q}-A_{22,q})\\
&\quad+\cos(2\phi_q)(A_{22,q}-A_{11,q})],\\
B_{y,q}&=\frac{1}{2}\sin\theta_q\sin(2\phi_q)(A_{22,q}-A_{11,q}).
\end{aligned} \tag{2}$$

For an axially symmetric hyperfine interaction, A_q and B_q are related to the principal values $A_{\perp,q}$ and $A_{\parallel,q}$ of the hyperfine tensor and can be expressed as function of the isotropic and dipolar hyperfine coupling constants, $a_{\mathrm{iso},q}$ and T_q, by

$$\begin{aligned}
A_q&=A_{\parallel,q}\cos^2\theta_q+A_{\perp,q}\sin^2\theta_q=T_q(3\cos^2\theta_q-1)+a_{\mathrm{iso},q},\\
B_q&=3T_q\sin\theta_q\cos\theta_q,
\end{aligned} \tag{3}$$

where θ_q is the angle between the external magnetic field and the electron–nucleus axis [1].

The resonance frequencies of nucleus q associated with the $\alpha(m_S=+\frac{1}{2})$ and $\beta(m_S=-\frac{1}{2})$ electron spin manifolds are

$$\omega_{\alpha,\beta,q}=\sqrt{(\omega_{I,q}\pm A_q/2)^2+(\pm B_q/2)^2}. \tag{4}$$

The pseudo-secular part B_q of the hyperfine tensor tilts the quantization axes of the nuclear spins for each m_S manifold by an angle

$$\eta_{\alpha,\beta,q}=\arctan\frac{\pm B_q/2}{\omega_{I,q}\pm A_q/2} \tag{5}$$

with respect to $\boldsymbol{B}_0$. The half-angle between the two nuclear quantization axes is given by $\eta_q=(\eta_{\alpha,q}-\eta_{\beta,q})/2$. The modulation depth parameter k_q, a fundamental quantity of ESEEM, is

$$k_q=\sin^2(2\eta_q)=\left(\frac{B_q\omega_{I,q}}{\omega_{\alpha,q}\omega_{\beta,q}}\right)^2 \tag{6}$$

with $0\leqslant k_q\leqslant 1$. It is a measure of the degree of dissimilarity of the nuclear sublevels in the α and the β electron manifolds.

The behavior of the spin system during a pulse sequence is described by the evolution of the density operator σ [1,14–16]. The density operator at a time t is given by

$$\sigma(t)=\ldots P_2Q_{t_1}P_1\sigma_0P_1^{-1}Q_{t_1}^{-1}P_2^{-1}\ldots \tag{7}$$

where P_j represent pulse propagators and Q_{t_j} free evolutions. In the ideal pulse approximation, the static Hamiltonian H_0 is neglected during the microwave pulse, so that

$$P_j=\mathrm{e}^{-\mathrm{i}\beta_jS_{x(y)}} \tag{8}$$

is the propagator for a pulse with flip angle β_j and phase $x(y)$. The propagator during free evolution is

$$Q_{t_j}=U^{\dagger}\mathrm{e}^{-\mathrm{i}H_0^{\mathrm{diag}}t_j}U \tag{9}$$

with [1]

$$H_0^{\mathrm{diag}}=UH_0U^{\dagger}\qquad U=\prod_{q=1}^{N_I}\mathrm{e}^{-\mathrm{i}(\eta_{\alpha,q}S_{\alpha}+\eta_{\beta,q}S_{\beta})I_{y,q}}. \tag{10}$$

At the beginning of the pulse sequence, the system is at thermal equilibrium. Conventionally, this is represented by $\sigma_0=-S_z/M$, where $M=\prod_q(2I_q+1)$ is the total num-

ber of nuclear sub-states per electron manifold. In order to simplify our calculations we use

$$\sigma_0 = \frac{1}{M} S_\beta = \frac{1}{M}\left(\frac{1}{2}\mathbb{I} - S_z\right) \tag{11}$$

instead. Adding to σ_0 a term proportional to the unity operator $\mathbb{I}$ does not affect the expectation value of S_+ as the unity operator is invariant during the pulse sequence and $\mathrm{tr}[S_+(c\mathbb{I} + \sigma)] = \mathrm{tr}[S_+\sigma]$ is satisfied.

The measured signal is given by the expectation value of the detection operator $S_+ = S_x + \mathrm{i}S_y$ at the time of the echo maximum, which is

$$E = \langle S_+ \rangle = \mathrm{tr}[S_+\sigma_{\mathrm{echo}}]. \tag{12}$$

If we write the density operator in the electron eigenbasis in terms of four $M \times M$ submatrices,

$$\sigma = \begin{pmatrix} \sigma_\alpha & \sigma_+ \\ \sigma_- & \sigma_\beta \end{pmatrix} \tag{13}$$

the signal can be written as $\langle S_+ \rangle = \mathrm{tr}(\sigma_-)$. The submatrices describe magnetization with different electron coherence orders [17,18]. The off-diagonal blocks σ_+ and σ_- represent electron coherence orders $p = +1$ (hereafter $+$) and $p = -1$ (hereafter $-$), corresponding to magnetization rotating in a plane perpendicular to the external field. When having one of these coherence orders, spins acquire a phase of $\exp(-\mathrm{i}p\Omega_S t)$ during free evolution. Components corresponding to polarization or nuclear coherence ($p = 0$) are distinguished for the two electronic manifolds: σ_α and σ_β represent electron coherence order of zero in the α and β electron manifold, symbolized by 0_α and 0_β, respectively. These correspond to magnetization parallel and antiparallel to the external field. Each of the four submatrices with particular *electron* coherence order consists of a set of components with different *nuclear* coherence orders, which give rise to separate ESEEM peaks [18].

Microwave pulses transfer and redistribute magnetization among the four density submatrices and thus change the electron coherence order. At the time of the echo, the total density matrix is a sum over components that have experienced different electron coherence orders during the various free evolution periods in the pulse sequence. In this way a pulse sequence with P periods of free evolution is characterized by N_σ particular electron coherence transfer pathways (eCTPs), i.e. N_σ sets of electron coherence levels $(p_0, p_1, \ldots, p_P)$ during the free evolution times $(t_1, \ldots, t_P)$, where p_0 is the electron coherence order at thermal equilibrium and p_j the electron coherence order during the free evolution time t_j after the jth pulse. Each eCTP starts at $p_0 = 0_\beta$ because of Eq. (11), and ends in observable $p_P = -1$ coherence if using quadrature detection. For simplicity, we will omit p_0 in the following. A detailed description how to select one or several eCTPs by phase cycling can be found elsewhere [16,17,19].

The density matrix at the time of the echo (Eq. (7)) and the expectation value $\langle S_+ \rangle$ (Eq. (12)) are sums of contributions from all possible eCTPs. In the ideal pulse approximation, each density matrix corresponding to a particular pathway can be written as a tensor product of density submatrices of single-nucleus subsystems, so that the eCTP signal from a multi-nuclear spin system is a product of signals from spin systems with one nucleus each. Summing over all contributing eCTPs, we get

$$E = \sum_{i=1}^{N_\sigma} \zeta_i \prod_{q=1}^{N_I} E_q^{(i)}, \tag{14}$$

where E is the total signal from the multinuclear spin system, ζ_i is a pathway-specific phase factor depending on pulse phases, and $E_q^{(i)}$ represents the signal from pathway i for a spin system containing one nucleus q only. The first $(\pi/2)$-pulse of a pulse sequence generates eCTPs starting with $p_1 = +1$ and with $p_1 = -1$. The prefactor ζ_i is necessary, because the nuclear-coherence generator of 5-pulse ESEEM and 6-pulse HYSCORE, $(\pi/2)_y - \tau_1 - (\pi)_y - \tau_1 - (\pi/2)_x$, transfers eCTPs starting with $(+,-)$ *and* eCTPs starting with $(-,+)$ into detecteable pathways. Eq. (14) represents a generalized product rule [8,20,21], which allows to compute ESEEM signals of multi-nuclear spins systems from those of single-nucleus spin systems for an arbitrary pulse sequence. Details will be discussed elsewhere (S. Stoll, in preparation).

An echo is formed when the spins have spent equal amounts of time as $p_j = +1$ and $p_j = -1$ coherence, so that the total accumulated phase is zero for all spins, independent of their particular Ω_S. Only a few of all possible pathways refocus, and in the computation of the ESEEM signal, only these pathways have to be taken into account. If the density matrix is not treated on a per-pathway basis, an integration over an inhomogeneous distribution of Ω_S is necessary [8].

The echo signal $E(t_1, t_2, \ldots)$ is a function of the interpulse delays. In order to estimate k [8], the signal is usually normalized by dividing it by the signal at zero evolution times, $E(0, 0, \ldots)$. This gives a normalization constant which contains $1/N_\sigma$, where N_σ is the number of pathways contributing to the echo. As we are interested in comparing *absolute* ESEEM signal intensities from sequences with different numbers of echo-forming pathways, we will omit this N_σ normalization in this paper.

3. Experimental

Experiments to illustrate the theoretically predicted behavior have been carried out using a degassed solution of 5 mM ^{63}Cu(Gly-$^{13}C_2$)$_2$ with 110 mM glycine in 4:6 water/glycerol, where the pH was adjusted to 7.3 with KOH [22,23].

All pulse EPR spectra were recorded on an X-band Bruker ELEXSYS E680 spectrometer at a magnetic field of $B_0 = 337.6$ mT and a temperature of $T = 20$ K. The pulse sequences employed are shown in Fig. 1. Pulse lengths of 12 ns for $\pi/2$ pulses and 24 ns for π pulses were used for all experiments, with $T_0 = 48$ ns and an increment of

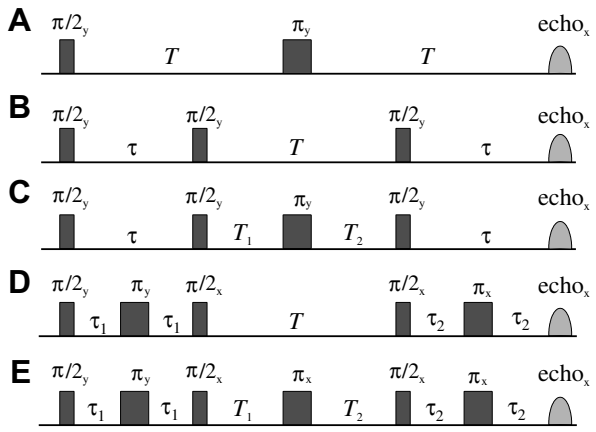

Fig. 1. ESEEM pulse sequences (variable T, T_1, T_2 and fixed τ, τ_1, τ_2): (A) 2-pulse ESEEM, (B) 3-pulse ESEEM, (C) standard (4-pulse) HYSCORE, (D) 5-pulse ESEEM, (E) 6-pulse HYSCORE.

$\Delta T = 12$ ns. In order to make signals from the various pulse sequences quantitatively comparable, the number of scans was set so as to keep the acquisition time identical in combination with the number of phase-cycle steps. A 4-step phase cycle was used for 3- and 4-pulse ESEEM. In order to handle the pulse phases correctly $(+\pi/2)_x$-pulses were tuned such that the imaginary part signal reaches a maximized and positive primary echo, $(+\pi/2)_y$-pulses such that the real part signal reaches a maximized and negative primary echo. A 2-step phase cycle was used for the 5-pulse ESEEM measurements and a 4-step phase cycle for 6-pulse HYSCORE. Details of these phase cycles are relegated to Appendix A. The data processing was kept the same in order to be able to quantitatively compare the intensities obtained by the various pulse sequences.

4. 1D experiments: 2-, 3- and 5-pulse ESEEM

4.1. One nucleus

Before comparing 3-pulse and 5-pulse ESEEM for multinuclear spin systems, we start by discussing basic properties of these one-dimensional ESEEM experiments for the case of one nucleus, based on the theory outlined in Section 2. We omit the nuclear index q.

For completeness and future reference we first look at the 2-pulse ESEEM experiment as shown in Fig. 1A. The only eCTP contributing to the 2-pulse echo is $(+,-)$. The signal due to this pathway is [24]

$$E_{2p}(T) = \left(1 - \frac{k}{2}\right) + \frac{k}{2}\left(\cos(T\omega_\alpha) + \cos(T\omega_\beta) - \frac{1}{2}\cos(T\omega_-) - \frac{1}{2}\cos(T\omega_+)\right) \quad (15)$$

with $\omega_\pm = \omega_\alpha \pm \omega_\beta$. Unlike the other ESEEM sequences discussed in this paper, 2-pulse ESEEM yields sum and difference peaks, at ω_+ and ω_-, respectively, inverted and with half the intensity of the basic peaks at ω_α and ω_β. The peak amplitudes of 2-pulse ESEEM are determined by the modulation depth parameter k only, whereas additional factors contribute to the amplitudes of the other ESEEM sequences shown in Fig. 1.

As there is only one echo pathway in 2-pulse ESEEM ($N_\sigma = 1$), the product rule Eq. (14) for a multi-nuclear system consists of a single product of signals from the N_I one-nucleus subsystems [24],

$$E_{2p}(T) = \prod_{q=1}^{N_I} E_{2p,q}. \quad (16)$$

The 3-pulse ESEEM experiment [8] is shown in Fig. 1B. The eCTPs contributing to the echo of the 3-pulse ESEEM experiment are $(+,0_\alpha,-)$ and $(+,0_\beta,-)$. The signal is the sum of the evolutions of nuclear coherences in the α and in the β manifold, with the α pathway signal

$$E^\alpha_{3p}(T;\tau) = (1 - kb^\alpha_{3p}) + kb^\alpha_{3p}\cos((T+\tau)\omega_\alpha) \quad (17)$$

and the blind-spot term

$$b^\alpha_{3p} = \sin^2\left(\frac{\tau\omega_\beta}{2}\right) \quad (18)$$

and E^β_{3p} analogous by exchanging α and β. Peaks appear at ω_α and ω_β, and their amplitudes are proportional to the modulation depth parameter k and to the τ-dependent blind-spot term b^α_{3p}.

The fact that two pathways contribute to the echo ($N_\sigma = 2$), is also reflected by the product rule [20]

$$E_{3p}(T;\tau) = \prod_{q=1}^{N_I} E^\alpha_{3p,q} + \prod_{q=1}^{N_I} E^\beta_{3p,q}, \quad (19)$$

where we have, as announced, omitted the N_σ normalization factor 1/2.

The 5-pulse ESEEM sequence [6] is shown in Fig. 1D. It differs from the remote-echo detected 2-pulse ESEEM [25] only in the choice of pulse phases and in the interpulse delay incrementation. Four eCTPs contribute to the 5-pulse echo: $(+,-,0_\alpha,+,-)$, $(-,+,0_\alpha,+,-)$, $(+,-,0_\beta,+,-)$ and $(-,+,0_\beta,+,-)$, which we abbreviate with α_+, α_-, β_+ and β_-, respectively. The modulation expressions for the two α pathways are

$$E^{\alpha_\pm}_{5p}(T;\tau_1,\tau_2) = E_{2p}(\tau_1)E_{2p}(\tau_2) \mp b_{5p}\Big[-4k^2C^\alpha_0 + 4k\cos^4\eta\cos(T\omega_\alpha + \phi_{\alpha_+} + \phi_{\beta_+}) + 2k^2\cos\phi_{\beta_-}\cos(T\omega_\alpha + \phi_{\alpha_+}) + 4k\sin^4\eta\cos(T\omega_\alpha + \phi_{\alpha_+} - \phi_{\beta_+})\Big] \quad (20)$$

with

$$C^\alpha_0 = \cos\left(\frac{\tau_1\omega_\alpha}{2}\right)\cos\left(\frac{\tau_2\omega_\alpha}{2}\right)\sin\left(\frac{\tau_1\omega_\beta}{2}\right)\sin\left(\frac{\tau_2\omega_\beta}{2}\right),$$
$$b_{5p} = \sin\left(\frac{\tau_1\omega_\alpha}{2}\right)\sin\left(\frac{\tau_2\omega_\alpha}{2}\right)\sin\left(\frac{\tau_1\omega_\beta}{2}\right)\sin\left(\frac{\tau_2\omega_\beta}{2}\right), \quad (21)$$

and the phase shifts $\phi_{\alpha\pm} = (\tau_1 \pm \tau_2)\ \omega_\alpha/2$ and $\phi_{\beta\pm} = (\tau_1 \pm \tau_2)\omega_\beta/2$. The expressions for the β pathways, $E^{\beta_\pm}_{5p}$, result by exchanging α and β in Eqs. (20) and (21).

The 5-pulse echo signal is a linear combination of the four pathway signals

$$E_{5p}(T;\tau_1,\tau_2) = E_{5p}^{\alpha_+} - E_{5p}^{\alpha_-} + E_{5p}^{\beta_+} - E_{5p}^{\beta_-}. \quad (22)$$

The two minus signs are a consequence of the pulse phases chosen (ζ_i in Eq. (14)).

It is remarkable that, in contrast to 2- and 3-pulse ESEEM, *two* pathways contribute to each peak in the 5-pulse ESEEM spectrum. The first, unmodulated term on the right-hand side of Eq. (20) (which is, interestingly, a product of two 2-pulse ESEEM modulations) cancels if the signals from the two pathways containing 0_α (or 0_β) are combined. The remaining unmodulated terms $-4k^2C_0^\alpha$ and $-4k^2C_0^\beta$ are usually small, so that the overall signal oscillates around $\approx$0.

The 5-pulse echo has x-phase. Orthogonal to it, with y-phase, appears the primary echo due to the last two pulses. This unmodulating echo increases with the free evolution time T, as magnetization from the 5-pulse ESEEM eCTPs relaxes into the eCTP $(0,0,0,+,-)$, i.e. the primary echo. Therefore the signal with y-phase allows to determine the relaxation time T_1.

Eq. (20) is compact and general. Gemperle [26] gives a much longer, slightly incorrect expression.[2] The formulas in other publications are restricted to the special case $\tau_1 = \tau_2 = \tau$ [1,6] and to small values of η [27].

For systems with more than one nucleus, the product rule for 5-pulse ESEEM includes four terms, one for each pathway:

$$E_{5p}(T;\tau_1,\tau_2) = \prod_{q=1}^{N_I} E_{5p,q}^{\alpha_+} - \prod_{q=1}^{N_I} E_{5p,q}^{\alpha_-} + \prod_{q=1}^{N_I} E_{5p,q}^{\beta_+} - \prod_{q=1}^{N_I} E_{5p,q}^{\beta_-}. \quad (23)$$

As the modulation in the 5-pulse ESEEM signal consists of several terms with different amplitudes and phases, it is difficult to generally compare it to 3-pulse ESEEM. However, some basic properties can be inferred by examining the dependence of Eq. (20) on η (k) and τ_1, τ_2 separately.

After summing over the two contributing pathways, the τ_1- and τ_2-independent amplitude pre-factors[3] in the 5-pulse ESEEM expression in Eq. (20) are

$$a_{5p,1} = 8k\cos^4\eta \quad a_{5p,2} = 4k^2 \quad a_{5p,3} = 8k\sin^4\eta. \quad (24)$$

As they are nonlinear in k, they are clearly different from 3-pulse ESEEM, where the τ-independent part of the amplitude, $a_{3p} = k$ (Eq. (17)), is linear in k. The dependence of the various amplitude factors on η and k is shown in Fig. 2.

The modulation amplitude for a weakly coupled nucleus ($\eta \approx 0$, $k \ll 1$) is mainly determined by the first term, $a_{5p,1}$. This term is about 8 times larger than a_{3p}, so that the modulation depth is considerably enhanced compared to the 3-pulse experiment [6]. In the strong coupling case ($\eta \approx \pi/2$, $k \ll 1$), the third term dominates and yields similarly an eightfold modulation enhancement.

For nuclei in the intermediate coupling regime ($\eta \approx \pi/4$, $k \approx 1$), all three terms contribute significantly to the amplitude, and the effective modulation enhancement depends on the relative phases between them, which are dependent both on τ_1 and τ_2 and on ω_α and ω_β and can lead to constructive or destructive interference. In the case $\eta = \pi/4$ ($k = 1$), the modulating parts of Eq. (20) reduce to

$$\mp b_{5p} \cdot 4\cos(T\omega_\alpha + \phi_{\alpha_+})\cos(\omega_\beta\tau_1/2)\cos(\omega_\beta\tau_2/2), \quad (25)$$

thus yielding an effective amplitude pre-factor of

$$8\cos(\omega_\beta\tau_1/2)\cos(\omega_\beta\tau_2/2). \quad (26)$$

Although this pre-factor indicates an eightfold increase in intensity compared to 3-pulse ESEEM, the interference of the three signal contributions leads to two additional τ_1- and τ_2-dependent suppression factors, which will significantly reduce the peak amplitude. The magnitude of this additional suppression can be anywhere between 0 and 1, its average over all possible τ_1 and τ_2 is $4/\pi^2 \approx 0.4$. The total amplitude in this intermediate coupling regime can therefore vary strongly, and the modulation can be deeper or shallower compared to the 3-pulse case, in contrast to the $k \approx 0$ regions, where the enhancement is generally substantial.

This improvement of the modulation depth in 5-pulse ESEEM as compared to 3-pulse ESEEM is reduced due

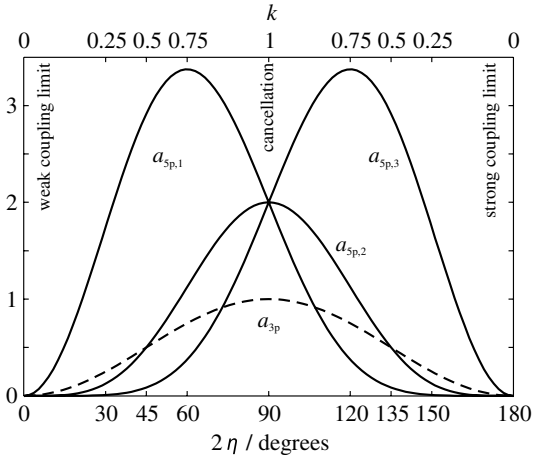

Fig. 2. 3-pulse and 5-pulse ESEEM amplitudes of the ω_α and ω_β peaks as function of η and k, for $b_{3p}(\tau) = b_{5p}(\tau_1,\tau_2) = 1$. $a_{5p,1} = 8\ k\cos^4\eta$, $a_{5p,2} = 4k^2$ and $a_{5p,3} = 8k\ \sin^4\eta$; $a_{3p} = k$.

[2] An additional factor of 2 for the *constant* part of the 5-pulse ESEEM formula is obtained in our recalculation, while the *modulating* part of the 5-pulse ESEEM formula [6,26,27] corresponds to our result (apart from the N_σ normalization). We therefore were able to reproduce earlier conclusions (including the discussion for the special case $\tau = \tau_c$ and for small values of k and η). The relation of our formula to the 5-pulse ESEEM formula as in Ref. [1] is yet unclear. Our recalculation of the 3-pulse ESEEM intensity of the α SQ peak, after including the $N_\sigma = 2$ factor, results in $A_\alpha(\tau_c) = kb_{3p}^\alpha(\tau_c)/2 = k/2$ and is different from $A_\alpha(\tau_c) \equiv E_\alpha^{3p}(\tau_c) = k/4$ [6,26,27]. Hence, an improvement of the α SQ peak amplitude by a factor of 8 for small values of k if using 5-pulse ESEEM instead of 3-pulse ESEEM can only be obtained if the N_σ normalizations are omitted.

[3] The dependence of amplitude pre-factors on τ can be omitted from discussion, when the blind spots fulfill $\tau_c = (1+2l)\pi/\omega_{\alpha,\beta}$ where l is a positive integer. Then blind spot factors become $b_{3p}^{\alpha,\beta}(\tau_c) = b_{5p}(\tau_{1c},\tau_{2c}) = 1$.

to transversal relaxation and off-resonance effects [6]. The effective sensitivity enhancement under experimental conditions is therefore difficult to predict: improvement factors between 2 [6] and 8 [27] were reported. However, an improvement of a factor two still leads to considerably better spectra of low-concentration protein samples where the S/N ratio is critical.

The other factors determining the amplitudes of 3-pulse and 5-pulse ESEEM peaks are the blind-spot terms in Eqs. (18) and (21). A fundamental difference is apparent: while the ω_α and ω_β peak intensities in 3-pulse ESEEM depend on different blind-spot terms, b_{3p}^{α} and b_{3p}^{β}, respectively, the 5-pulse ESEEM blind-spot term b_{5p} is the same for both spectral peaks. Unlike 3-pulse ESEEM spectra, 5-pulse ESEEM spectra of $I = 1/2$ nuclei with small k are therefore symmetric. This constitutes an advantage of 5-pulse over 3-pulse ESEEM, as it facilitates spectral interpretation. For large k, the additional suppression factor of the second term in Eq. (20) destroys this symmetry. The 5-pulse ESEEM modulation expression is also symmetric with respect to an interchange of τ_1 and τ_2.

The 5-pulse ESEEM blind-spot term in Eq. (21) can be written as a combination of 3-pulse ESEEM blind-spot terms

$$|b_{5p}(\tau_1,\tau_2)| = \sqrt{b_{3p}^{\alpha}(\tau_1)b_{3p}^{\beta}(\tau_1)b_{3p}^{\alpha}(\tau_2)b_{3p}^{\beta}(\tau_2)}. \quad (27)$$

If the two τ values are equal, $\tau_1 = \tau_2 = \tau$, the expression reduces to $b_{5p}(\tau,\tau) = b_{3p}^{\alpha}(\tau)b_{3p}^{\beta}(\tau) = b_{4p}^{2}(\tau)$, the square of the HYSCORE blind-spot term (see Section 5). If we additionally assume $\omega_\alpha \approx \omega_\beta \approx \omega_I$, which is valid for small hyperfine couplings (and hence small η), then $b_{3p}^{\alpha} \approx b_{3p}^{\beta}$, and the blind-spot term of 5-pulse ESEEM reduces to a squared 3-pulse ESEEM blind-spot term $b_{5p}(\tau,\tau) \approx b_{3p}^{2}(\tau) = \sin^4(\tau\omega_I/2)$. In this limit, the blind spots in 5-pulse ESEEM have the same location as in 3-pulse ESEEM, and no additional blind spots are created. The $b_{5p} \approx 1$ regions in 5-pulse ESEEM are narrower, and the blind spots are more pronounced, so that b_{5p} is more selective than b_{3p}. With finite pulse lengths, the blind spot behavior is more diffuse, and the difference between 3-pulse and 5-pulse ESEEM blind spots becomes less pronounced.

In practice, the choice of $\tau_1 = \tau_2$ is of importance to average out blind spots, as it is done at several τ in 3-pulse ESEEM. It is sufficient to acquire 5-pulse ESEEM spectra at several $\tau_1 = \tau_2$, a modulation which is described by $E_{5p}(T;\tau,\tau)$ (see Eqs. (20) and (21)). Averaging out blind spots at several $\tau_1 \neq \tau_2$ while keeping τ_2 constant is more demanding but also possible.

Experimental peak intensities of ^{63}Cu(Gly-$^{13}C_2$)$_2$ as a function of the two τ values are shown in Fig. 3. This system contains several weakly coupled protons and moderately modulating ^{13}C. It is relatively simple, as only $I = 1/2$ nuclei are visible in the ESEEM spectra.

The close relation of the 5-pulse ESEEM blind-spot term as compared to 3-pulse ESEEM for $\omega_\alpha \approx \omega_\beta$ is demonstrated in Fig. 3A and C. Fig. 3C shows the 3-pulse ESEEM blind-spot term $b_{3p}(\tau)$ acting on the ^{1}H matrix peak centered at 14.4 MHz. Fig. 3A illustrates the periodicity of the proton matrix peak due to $b_{5p}(\tau_1,\tau_2) = b_{3p}(\tau_1)b_{3p}(\tau_2)$ with $b_{5p}(\tau,\tau) = b_{3p}^{2}(\tau)$ on the diagonal line. Each point in Fig. 3A corresponds to the matrix peak amplitude of a 5-pulse ESEEM spectrum. The 5-pulse ESEEM intensities of the ^{1}H matrix peak are on average about twice the 3-pulse ESEEM intensities shown in Fig. 3C.

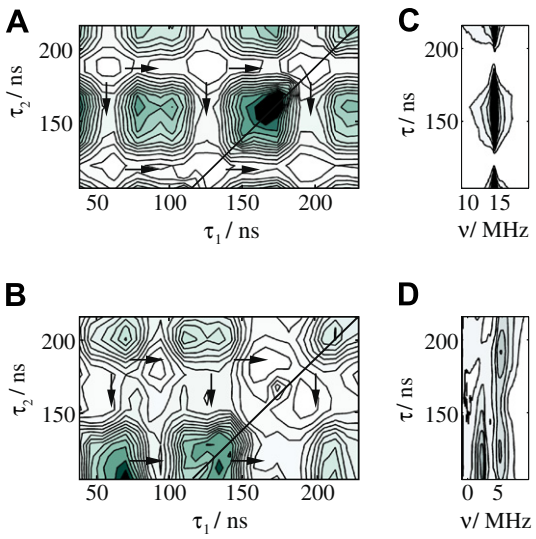

Fig. 3. Measured peak intensities of ^{63}Cu(Gly-$^{13}C_2$)$_2$ at $T = 20$ K and $B_0 = 337.6$ mT. The diagonal lines mark $\tau_1 = \tau_2$, arrows point to the centers of "blind zones", see text for details. (A) 5-pulse ESEEM ^{1}H matrix peak intensities, at 14.4 MHz, as a function of (τ_1,τ_2). (B) 5-pulse ESEEM ^{13}C peak intensities, summed over 0–8.3 MHz as a function of (τ_1,τ_2). (C) 3-pulse ESEEM spectra as a function of τ, 9–20 MHz. (D) 3-pulse ESEEM spectra as a function of τ, 0–8.3 MHz.

In general, the α- and β-single-quantum (SQ) peaks are found at different frequencies ω_α and ω_β. The blind-spot behavior for the two ^{13}C frequencies $\omega_{\alpha,^{13}C} \neq \omega_{\beta,^{13}C}$ is illustrated in Fig. 3B and D. The SQ-peak amplitudes are clearly different for the two SQ-peak amplitudes in 3-pulse ESEEM (Fig. 3D), in addition, these amplitudes are oscillating with two different blind-spot terms $b_{3p}^{\alpha}(\tau)$ and $b_{3p}^{\beta}(\tau)$ (Eqs. (17)-(18)). The blind-spot term of 5-pulse ESEEM (Eqs. (21) and (27)) is the same for both SQ peaks. Each point in Fig. 3B represents the integral of the signal over the frequency range 0–8.3 MHz in a 5-pulse ESEEM spectrum, and contains the amplitude of both ^{13}C SQ-peaks. On the diagonal, where $\tau_1 = \tau_2$, these amplitudes are easily comparable to 3-pulse ESEEM described by $b_{5p}(\tau,\tau) = b_{3p}^{\alpha}(\tau)b_{3p}^{\beta}(\tau)$ (see also Fig. 3D). This recorded 5-pulse ESEEM blind spot behavior for any τ_1 and τ_2 is well described by Eq. (27). Also, the expected symmetry of the peak intensities with respect to an interchange of τ_1 and τ_2 is visible.

"Blind zones", i.e. areas in the (τ_1, τ_2)-plane where the modulation of all nuclei is simultaneously almost completely suppressed, can appear in 5-pulse ESEEM (marked

with arrows in Fig. 3A and B). Blind zones can be found by selecting one τ value in a blind-spot and another one in an anti-blind spot position of an arbitrary peak, for example the ^{1}H matrix peak. These zones can be avoided if measuring at $\tau_1 = \tau_2$ only. Nevertheless, the τ values *can* be chosen such that $\tau_1 \neq \tau_2$ in order to selectively enhance and suppress peaks more efficiently as in the special case $\tau_1 = \tau_2$; this capacity is of importance for further reducing the impact of the cross-suppression effect.

4.2. Multiple nuclei

The ESEEM signals of multi-nuclear spin systems are obtained from single-nucleus signals using the product rule in Eq. (14). As the signals from the individual nuclei are combined in a product rather than a sum, the nuclear peaks at the SQ frequencies ω_α and ω_β are reduced in intensity. This cross-suppression effect is a consequence of the product rule and is a disturbing effect in 3-pulse ESEEM [4] and HYSCORE [5,28,29] spectra of more than one nucleus coupled to same electron spin, resulting in reduced SQ-peak intensities and inter-nuclear combination peaks. Cross suppression only is negligible if all nuclei have $k \approx 0$. The SQ-peak amplitudes are then not affected by other nuclei. As a consequence, one can neglect higher order terms of k and any single-nucleus modulation formula of the form $1 - k_q f_q(\omega_{\alpha,q}, \omega_{\beta,q})$ results in a superposition of the signals of each nucleus [1], i.e. $\prod_q 1 - k_q \cdot f_q(\omega_{\alpha,q}, \omega_{\beta,q}) \approx 1 - \sum_q k_q \cdot f_q(\omega_{\alpha,q}, \omega_{\beta,q})$. We will show that the above simplification is not only applicable to 2-pulse ESEEM (Eq. (15)) and 3-pulse ESEEM (Eq. (17)), but to all pulse sequences discussed here, assuming the special case of shallow modulations only.

The 3-pulse ESEEM intensity of the α SQ peak of a nucleus q at $\omega_{\alpha,q}$ is given by [4]

$$A_{\alpha,q}^{(\mathrm{eff.})} = A_{\alpha,q} \prod_{r \neq q} (1 - A_{\alpha,r}), \tag{28}$$

i.e. the amplitude in the single nucleus case $A_{\alpha,q} = k_q b_{3\mathrm{p},q}^{\alpha}$ is reduced by the amplitude of other nuclei r, leading to the effective amplitude $A_{\alpha,q}^{(\mathrm{eff.})}$ in a multi-nuclear spin system. This formula holds also when exchanging α and β. The reduction in the effective amplitude is large if any of the zero-frequency components $1 - A_{\alpha,r}$ is small, that is, when any $A_{\alpha,r} \approx 1$. This means that nuclei with large peak amplitudes (because of $k \approx 1$ and/or large blind-spot terms, see Eq. (17)) are strong suppressors that reduce the SQ peak intensity of other nuclei significantly. This is a consequence of the fact that a given total electron spin polarization feeds all nuclear coherences, so that strong branching towards one particular coherence necessarily diminishes the amplitude of other coherences.

Such nuclei include ^{14}N, which often is in the $k \approx 1$ regime at X-band frequencies [30], ^{13}C and ^{2}H. The cross suppression can seriously affect intensities of ^{1}H peaks in partially deuterated samples and impede a correct interpretation when comparing them with spectra from non-deuterated samples, which is a common way of assigning ^{1}H ESEEM peaks. The more suppressors are present in a spin system, the larger the cross suppression on nuclei with inherently weak ESEEM intensities. The cross suppression of weak SQ peaks in 3-pulse ESEEM can only be alleviated by enhancing $A_{\alpha,q}$ and/or reducing the amplitudes $A_{\alpha,r}$ of all suppressor nuclei as can be seen from Eq. (28). An appropriate choice of τ in the blind-spot term $b_{3\mathrm{p},q}^{\alpha}$ is one possibility.

The contributions to the SQ-peak amplitude at $\omega_{\alpha,q}$ in 5-pulse ESEEM, due to the eCTPs α_+ and α_-, respectively, are reduced by the zero-frequency components

$$\prod_{r \neq q} (E_{2\mathrm{p},r}(\tau_1) E_{2\mathrm{p},r}(\tau_2) \mp 4k_r^2 b_{5\mathrm{p},r} C_{0,r}^{\alpha}). \tag{29}$$

A detailed discussion is demanding due to the complexity of this expression. Still, some features are easily deduced. If $k_r \approx 0$ for all nuclei r the first term in Eq. (29) simplifies to $E_{2\mathrm{p},r}(\tau_1) E_{2\mathrm{p},r}(\tau_2) \approx 1$ while the second term vanishes. Then, the spectrum of a multi-nuclear spin system equals a superposition of the single-nucleus spectra, unaffected by cross suppression (Appendix B). Cross suppression due to the presence of $k_r = 1$ nuclei has the ability to reduce and conceal 5-pulse ESEEM peaks. But one has to keep in mind, that cross suppression now affects improved peak amplitudes (Section 4.1). The reduction of an SQ-peak amplitude in 5-pulse ESEEM spectra depends on τ_1 and τ_2. In 5-pulse ESEEM, as in 3-pulse ESEEM, cross suppression can be negligible even in the presence of strong suppressors due to the influence of the blind-spot terms. Eq. (29) therefore underlines the importance of recording 5-pulse ESEEM spectra at more than one blind spot position; not only to average out blind-spots, but also to avoid a potential cross-suppression effect. This result is valid particularly for $\tau_1 = \tau_2$, and—although experimentally more demanding—for $\tau_1 \neq \tau_2$. In 5-pulse ESEEM τ_2 is limited by the dead time, but by using remote echo detection [25] this can be overcome and the full (τ_1, τ_2) dependence of the signals can be exploited. The phase cycling for remote echo detected 5-pulse ESEEM is given in Appendix A.

The creation of inter-nuclear peaks at multi-quantum (MQ) frequencies, which are sums and differences of the SQ frequencies of various nuclei, also is a consequence of the product rule (14). This result is due the trigonometric property $\cos\phi_1 \cos\phi_2 = [\cos(\phi_1 + \phi_2) + \cos(\phi_1 - \phi_2)]/2$. As the total amplitude is conserved, the peak intensity that is distributed over these new MQ peaks is lost from the basic single-quantum (SQ) peaks and the unmodulated part.

In 3-pulse ESEEM, the amplitudes of the MQ peaks involve α SQ frequencies from N_{MQ} nuclei q_i, but not from the other nuclei p_j, are all equal and given by

$$A_{\alpha,q_1 \pm \alpha,q_2 \pm \ldots} = \frac{1}{2^{N_{\mathrm{MQ}}-1}} \cdot \prod_i A_{\alpha,q_i} \cdot \prod_j (1 - A_{\alpha,p_j}). \tag{30}$$

A similar expression holds for β MQ peaks, or for each pathway in general. These MQ peaks are created at $\sum_{i=1}^{N_{MQ}} \pm \omega_{\alpha,q_i}$ and $\sum_{i=1}^{N_{MQ}} \pm \omega_{\beta,q_i}$. If $N_{MQ} = 2$ this formula reduces to the one given in Ref. [4]. From all these MQ peaks only those containing linear combinations of frequencies from *two* nuclei, i.e. the zero-quantum $(\omega_{\alpha,q_1} - \omega_{\alpha,q_2})$ and double-quantum $(\omega_{\alpha,q_1} + \omega_{\alpha,q_2})$ peaks, are pronounced. Higher-order MQ peaks involving more than two nuclei are weaker, as the intensity of the inter-nuclear cross peaks scale with the inverse power of the order of the MQ-transition.

The product rules of 3- and 5-pulse ESEEM (Eqs. (19) and (23)) combine frequencies stemming from the same m_S manifold, whereas the product rule of 2-pulse ESEEM (Eq. (16)) contains a single eCTP for both m_S manifolds. The contribution of sum- and difference peaks to cross suppression in 2-pulse ESEEM further hinders a quantitative comparison with 5-pulse ESEEM. Due to these differences, cross-suppression in 2-pulse ESEEM is only briefly discussed and not compared to 5-pulse ESEEM. The effective SQ-peak intensities at $\omega_{\alpha,q}$ in 2-pulse ESEEM

$$A_{\alpha,q}^{(\text{eff.})} = k_q/2 \prod_{r \neq q} (1 - k_r/2), \tag{31}$$

reveal an improvement as compared to 3-pulse ESEEM. The reduction due to cross suppression, $1 - k_r/2$, has an upper limit of 1/2 for strong suppressors $k_r \approx 1$, in contrast to 3-pulse ESEEM where complete suppression is possible. Also the sum and difference peaks are reduced by $\prod_{r \neq q}(1 - k_r/2)$. In practice, a large number of suppressors can be present, and peak intensities of nucleus q might fall under the noise level. The lack of the blind-spot term gives no possibility to reduce the cross suppression on a nucleus with $k_q \approx 0$ in 2-pulse ESEEM. In fact, another experimentally adjustable parameter, the pulse length, overcomes this limit (see Ref. [31]). Also MQ peaks are created at large modulation depths k. These inter-nuclear cross peaks are MQ combinations between the α SQ, β SQ and sum- and difference peaks.

An exemplary simulation of 3-pulse and 5-pulse ESEEM of a $k \approx 0$ nucleus, ^{1}H, in the absence and the presence of a strong suppressor nucleus, ^{13}C, is shown in Fig. 4. In the absence of ^{13}C, the ^{1}H peaks in the 5-pulse spectrum are about 5 times as intense as in the 3-pulse spectrum. When the ^{13}C nucleus is included, the ^{1}H peaks in both 3-pulse and 5-pulse are reduced in intensity due to cross suppression. In the 3-pulse ESEEM, one of the two ^{1}H is almost missing, and two weak inter-nuclear combination peaks appear. The suppression in the 5-pulse ESEEM spectrum is the same for both ^{1}H peaks, and the relative intensity loss is small. In addition, no visible multi-quantum peaks are present. Closer examination of the signals resulting from Eqs. (20) and (23) reveals that the inter-nuclear coherences are present in all eCTPs, but have opposite phases in the two α (β) pathways, so that they cancel. This absence of MQ peaks is another advantage of 5-pulse ESEEM over 3-pulse ESEEM, as it simplifies potentially crowded spectra. MQ peaks can, however, be of diagnostic importance in some cases as their positions reveal relative signs of hyperfine interactions [28,29].

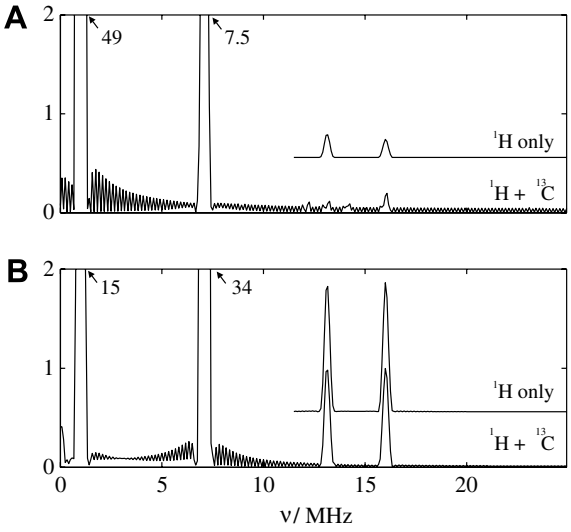

Fig. 4. Simulation of (A) 3-pulse ESEEM and (B) 5-pulse ESEEM spectra. Parameters: $B_0 = 329$ mT, $\tau = \tau_1 = \tau_2 = 100$ ns; $\Delta T = 20$ ns, 300 points; ^{1}H: $A/2\pi = 4.00$ MHz, $B/2\pi = 3.00$ MHz, $\omega_I/2\pi = 14.0$ MHz, $\omega_\alpha/2\pi = 16.1$ MHz, $\omega_\beta/2\pi = 12.1$ MHz, $k = 0.046$; ^{13}C: $A/2\pi = 7.00$ MHz, $B/2\pi = 1.00$ MHz, $\omega_I/2\pi = 3.52$ MHz, $\omega_\alpha/2\pi = 7.04$ MHz, $\omega_\beta/2\pi = 0.50$ MHz, $k = 1.0$.

The effect of cross suppression is studied on the recorded 3- and 5-pulse ESEEM spectra of fully ^{13}C-labeled ^{63}Cu(gly)$_2$ (Fig. 5, see also Fig. 3). As inter-nuclear cross peaks do not occur in 5-pulse ESEEM, experimental evidence for the large modulation depths that are associated with cross-suppression has to be demonstrated by the reduction of the SQ-peak amplitudes. The recorded intensities of the proton matrix peak, which were shown in Fig. 3A, are superimposed by the function describing the reduction due to cross suppression by ^{13}C (see Eq. (29)). As the modulation depth parameter $k_{^{13}C}$ is smaller than 1/2, i.e. a relatively weak suppressor, the necessary term to describe cross suppression is $E_{2p,^{13}C}(\tau_1)E_{2p,^{13}C}(\tau_2)$ and the second term is negligible. The starting points of the

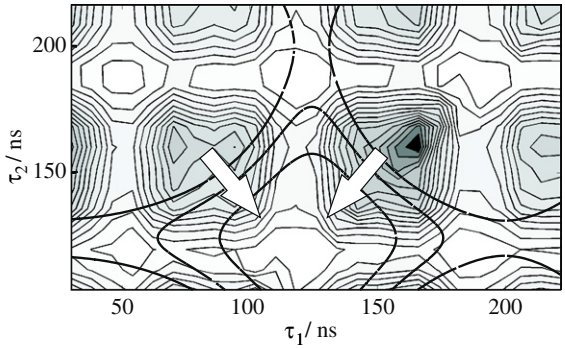

Fig. 5. Experimental 5-pulse ESEEM peak intensities of the proton matrix of ^{63}Cu(Gly-^{13}C$_2$)$_2$. $T = 20$ K and $B_0 = 337.6$ mT. Superimposed is the function describing the reduction due to cross-suppression by ^{13}C.

arrows in Fig. 5 indicate positions, where maximized SQ-amplitudes of the proton matrix would be expected due to the blind-spot term $b_{5p,^1H}$ in the absence of cross suppression. But the recorded maximal intensities are shifted towards higher τ_2 values, and lower and higher τ_1 values, respectively, as a larger reduction due to cross suppression is appearing towards $\tau_1 = \tau_2 \approx 125$ ns. A negligible cross suppression due to ^{13}C is found in the recorded 5-pulse ESEEM spectra if τ_2 is above 160 ns and τ_1 is either below 90 ns or above 160 ns. The relative intensity of the ^1H matrix peak as compared to the ^{13}C peaks was calculated for 3- and 5-pulse ESEEM at all blind spot positions, and revealed that this ratio is up to 7 times larger when using 5-pulse ESEEM instead of 3-pulse ESEEM. This shows that cross suppression can be avoided more efficiently when using 5-pulse ESEEM.

5. 2D experiments: 4- and 6-pulse HYSCORE

5.1. One nucleus

4-Pulse HYSCORE [9] is derived from 3-pulse ESEEM by adding a π mixing pulse during the evolution time T and incrementing the two resulting intervals T_1 and T_2 separately, so that a 2D signal is obtained (see Fig. 1C). The eCTPs contributing to the 4-pulse HYSCORE echo are $(+,0_\alpha,0_\beta,-)$ and $(+,0_\beta,0_\alpha,-)$, abbreviated as $\alpha\beta$ and $\beta\alpha$, yielding inter-manifold cross peaks correlating nuclear frequencies in the α and β electron manifolds, $(\omega_\alpha,\omega_\beta)$ and $(\omega_\beta,\omega_\alpha)$. In case of a non-ideal mixing pulse, contributions from the eCTPs $(+,0_\alpha,0_\alpha,-)$ and $(+,0_\beta,0_\beta,-)$ may also be present [17,32,33], resulting in intra-manifold cross peaks along the diagonal at $(\omega_\alpha,\omega_\alpha)$ and $(\omega_\beta,\omega_\beta)$. The modulation expression for 4-pulse HYSCORE as originally derived in [17,21] is given in Appendix C.

By a similar insertion of a π mixing pulse during T in the 5-pulse ESEEM sequence, a 6-pulse HYSCORE sequence as shown in Fig. 1E is obtained [7,34]. The 4 eCTPs contributing to the echo in this sequence are $(+,-,0_\alpha,0_\beta,+,-)$, $(-,+,0_\alpha,0_\beta,+,-)$, $(+,-,0_\beta,0_\alpha,+,-)$ and $(-,+,0_\beta,0_\alpha,+,-)$, abbreviated $\alpha\beta_+,\alpha\beta_-,\beta\alpha_+$ and $\beta\alpha_-$. They yield inter-manifold cross peaks as in 4-pulse HYSCORE. We were able to derive a relatively compact modulation formula for 6-pulse HYSCORE, for the case of ideal pulses. It is given in Appendix C. As in 4-pulse HYSCORE, if the mixing pulse is non-ideal, additional intra-manifold diagonal peaks might be present.

Apart from their dependence on the τ-dependent blind-spot term b_{4p}, the intensities of the 4-pulse HYSCORE cross peaks in the first quadrant, at $(\omega_\alpha,\omega_\beta)$ and $(\omega_\beta,\omega_\alpha)$, are determined by $a_{4p,1} = k\cos^2\eta$, whereas the second-quadrant cross peaks at $(\omega_\alpha,-\omega_\beta)$ and $(\omega_\beta,-\omega_\alpha)$ have an amplitude pre-factor $a_{4p,2} = k\sin^2\eta$ (see Eq. (44) and Fig. 6). The first term $a_{4p,1}$ dominates for nuclei in the weak coupling regime ($\eta \ll \pi/4$), whereas the second one dominates in the strong coupling regime ($\eta \gg \pi/4$). For intermediate coupling, both terms are of similar magnitude, and

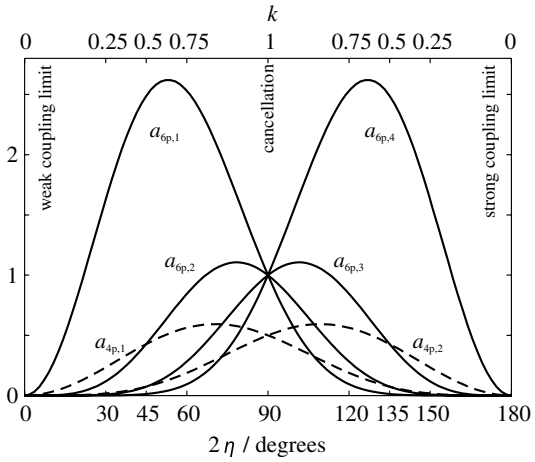

Fig. 6. 4-Pulse and 6-pulse HYSCORE amplitude terms for $b_{4p}(\tau) = b_{6p}(\tau_1,\tau_2) = 1$.

cross peaks both in the first and the second quadrant are visible. In disordered systems, peaks broaden into ridges [35], and destructive phase interference between signals from systems with similar orientations can lead to signal cancelation either in the first or second quadrant [36].

The blind-spot term in 4-pulse HYSCORE given in Eq. (48) (Appendix C) is related to the blind-spot terms of 3-pulse ESEEM by $b_{4p}^2 = b_{3p}^\alpha b_{3p}^\beta$. A detailed discussion of its impact on HYSCORE peak intensities can be found in [37].

6-Pulse HYSCORE cross-peak intensities, summed over the two $\alpha\beta$ (or $\beta\alpha$) pathways and at $\tau_{1,2}$-independent blind spots, have contributions from four terms with pre-factors

$$a_{6p,1} = 8k\cos^6\eta \quad a_{6p,2} = 2k^2\cos^2\eta, \\ a_{6p,3} = 2k^2\sin^2\eta \quad a_{6p,4} = 8k\sin^6\eta \tag{32}$$

as illustrated in Fig. 6. The terms $a_{6p,1}$ and $a_{6p,4}$ are dominant for weakly and strongly coupled nuclei, respectively, and give rise to peaks in the first and second quadrant, respectively. In these regimes, they are about eight times larger than the corresponding 4-pulse HYSCORE terms $a_{4p,1} = k\cos^2\eta$ and $a_{6p,2} = k\sin^2\eta$. In the intermediate coupling regime ($k > 0.5$), two additional terms become significant, each of them contributing to the peaks both in the first and the second quadrant. As all four terms are of similar magnitude, the total amplitude depends on the relative phases between these terms and is difficult to predict, but a behavior similar to the one discussed for 5-pulse ESEEM is expected, where the enhancement is on average substantially smaller than 8.

The blind-spot pre-factor in the 6-pulse HYSCORE modulation in Eq. (50) (Appendix C) is the same as for 5-pulse ESEEM, b_{5p} in Eq. (21), consequently the observations of Section 4 apply to 6-pulse HYSCORE, too.

5.2. Multiple nuclei

In 4-pulse HYSCORE, the presence of more than one modulating nucleus results in the appearance of a

multitude of cross peaks between MQ and MQ as well as MQ and SQ frequencies, while the cross suppression causes the original SQ/SQ cross peaks at ($\omega_{\alpha,q}$, $\omega_{\beta,q}$) etc. to loose intensity [4,5]. The effective amplitude of an SQ/SQ peak of nucleus q in a multi-nuclear spin system is

$$A_{\alpha,q}^{(\text{eff.})} = A_{\alpha,q} \cdot \prod_{r\neq q}\left(1 - k_r \frac{C_0^{(r)}}{4}\right), \tag{33}$$

where usually $A_{\alpha,q} \approx k_q b_{4\text{p}} \cos^2\eta_q$ and $C_0^{(r)}$ is given by Eq. (45) (Appendix C). In contrast to 3-pulse ESEEM, the cross-suppression effect on a SQ/SQ HYSCORE peak is not dependent on the blind-spot term, but on $C_0^{(r)}/4$, a quantity with values between 0 and 1.5. If $k_r \approx 0$ or $C_0^{(r)}/4 \approx 0$ for all nuclei, the effective single-quantum peak amplitudes remain as in the single-nucleus case. Nuclei $r \neq q$ having a value $0 \leqslant k_r C_0^{(r)}/4 \leqslant 1$ reduce the SQ/SQ peak amplitude of nucleus q, whereas nuclei with $1 < k_r C_0^{(r)}/4 \leqslant 1.5$ reduce and invert it. This sign change is without consequence in the usually displayed 4-pulse HYSCORE magnitude spectrum.

In 6-pulse HYSCORE, the part of the eCTP signal in Eq. (50) that is independent of T_1 and T_2 is responsible for the cross suppression. The reduction of the $\omega_{\alpha,q}$ SQ-peak amplitude due to the nuclei r, for the $\alpha\beta_+$ and $\alpha\beta_-$ contributions, respectively, is

$$\prod_{r\neq q}(E_{2\text{p},r}(\tau_1)E_{2\text{p},r}(\tau_2) \mp 4k_r^2 \cos(2\eta_r) b_{5\text{p},r} C_{0,r}). \tag{34}$$

The first term is the same as found in 5-pulse ESEEM (Eq. (29)), and simplifies to $E_{2\text{p},r}(\tau_1)\ E_{2\text{p},r}(\tau_2) \approx 1$ if all nuclei possess $k_r \approx 0$. The second term is negligible for small modulation depth parameters $k_r \ll 1$ of suppressing nuclei. The 6-pulse HYSCORE spectrum of a multi-nuclear spin system thus equals the superposition of the single-nucleus spectra, if all nuclei have $k_q \approx 0$. Due to the complexity of this term it is difficult to obtain further physical insight from the analytical equations. But with numerical simulations, the difference between 4-pulse and 6-pulse HYSCORE of a multi-nuclear spin system can be illustrated easily, as shown in Fig. 7. The 4-pulse experiment generates many MQ/MQ, SQ/MQ and MQ/SQ cross peaks in addition to the ^{1}H and ^{13}C SQ/SQ peaks. The ^{1}H SQ peaks are relatively weak and appear broadened, as the combination frequencies with the near-zero ^{13}C SQ frequency are very close to the ^{1}H SQ peak positions. In contrast, the 6-pulse HYSCORE ^{1}H peaks are sharper and significantly more intense.

It comes as no surprise that the peaks containing a combination frequency of the two nuclei are completely absent, just as was found earlier for 5-pulse ESEEM. Again, this is due to phase cancelation of the signals from the two eCTPs that contribute to the peak. 6-pulse HYSCORE spectra are therefore much simpler than the ones obtained in 4-pulse HYSCORE. Especially in systems with many strongly modulating nuclei, this can be of considerable help in the identification and assignment of peaks. Of course, MQ frequencies contain information which might be valuable after peaks have been assigned: The positions of MQ/MQ and MQ/SQ peaks reveal the relative sign of hyperfine coupling constants of different nuclei (see e.g. [38]). After understanding the 6-pulse HYSCORE spectrum it may thus be appropriate to measure 4-pulse HYSCORE to obtain this additional information.

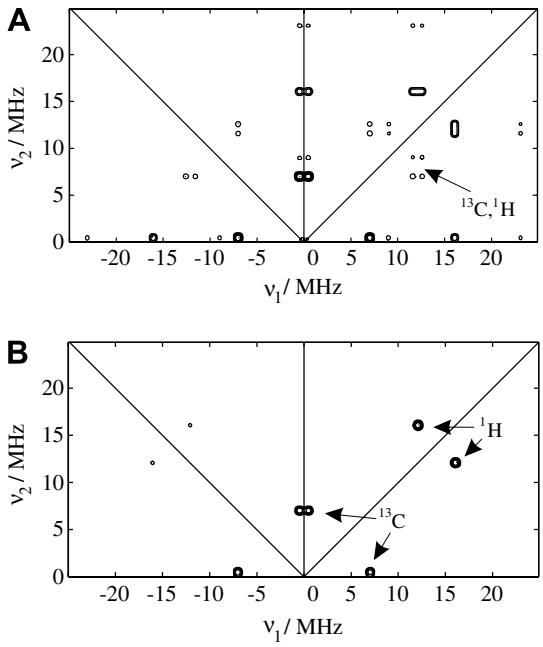

Fig. 7. Simulation of (A) 4-pulse HYSCORE, and (B) 6-pulse HYSCORE for a spin system containing one ^{1}H and one ^{13}C. Parameters as in Fig. 4.

The alleviated impact of the cross-suppression effect in 6-pulse HYSCORE can make it possible to observe signals from nuclei which are otherwise invisible. As an example, in Fig. 8 we show experimental 4-pulse and 6-pulse HYSCORE spectra of fully ^{13}C-labeled ^{63}Cu(Gly)$_2$, recorded under similar conditions (same total acquisition time). The ^{13}C and ^{1}H peaks are dominant in both HYSCORE spectra and of comparable intensity. Internuclear combination cross peaks are visible in the 4-pulse HYSCORE spectrum at $(\omega_{\alpha,^1\text{H}} \pm \omega_{\alpha,^{13}\text{C}}, \omega_{\beta,^1\text{H}} \pm \omega_{\beta,^{13}\text{C}})$. These peaks, marked with arrows in Fig. 8A, are MQ/MQ cross peaks between the ^{1}H matrix and the ^{13}C frequencies. Their positions are calculated by making use of the rather small modulation depth parameters for both nuclei ($k_{^1\text{H}} \ll k_{^{13}\text{C}} < 1/2$) at these experimental conditions, i.e. $a_{4\text{p},1}^{^1\text{H}}$ and $a_{4\text{p},1}^{^{13}\text{C}}$ are the dominant terms, and of the trigonometric property

$$\begin{aligned}
&\cos(T_1\omega_{\alpha,^1\text{H}} + T_2\omega_{\beta,^1\text{H}} + \phi_{^1\text{H}}) \\
&\quad\cdot \cos(T_1\omega_{\alpha,^{13}\text{C}} + T_2\omega_{\beta,^{13}\text{C}} + \phi_{^{13}\text{C}}) \\
&\quad= \frac{1}{2}[\cos(T_1(\omega_{\alpha,^1\text{H}} + \omega_{\alpha,^{13}\text{C}}) + T_2(\omega_{\beta,^1\text{H}} + \omega_{\beta,^{13}\text{C}}) \\
&\qquad+ \phi_{^1\text{H}} + \phi_{^{13}\text{C}}) + \cos(T_1(\omega_{\alpha,^1\text{H}} - \omega_{\alpha,^{13}\text{C}}) \\
&\qquad+ T_2(\omega_{\beta,^1\text{H}} - \omega_{\beta,^{13}\text{C}}) + \phi_{^1\text{H}} - \phi_{^{13}\text{C}})].
\end{aligned} \tag{35}$$

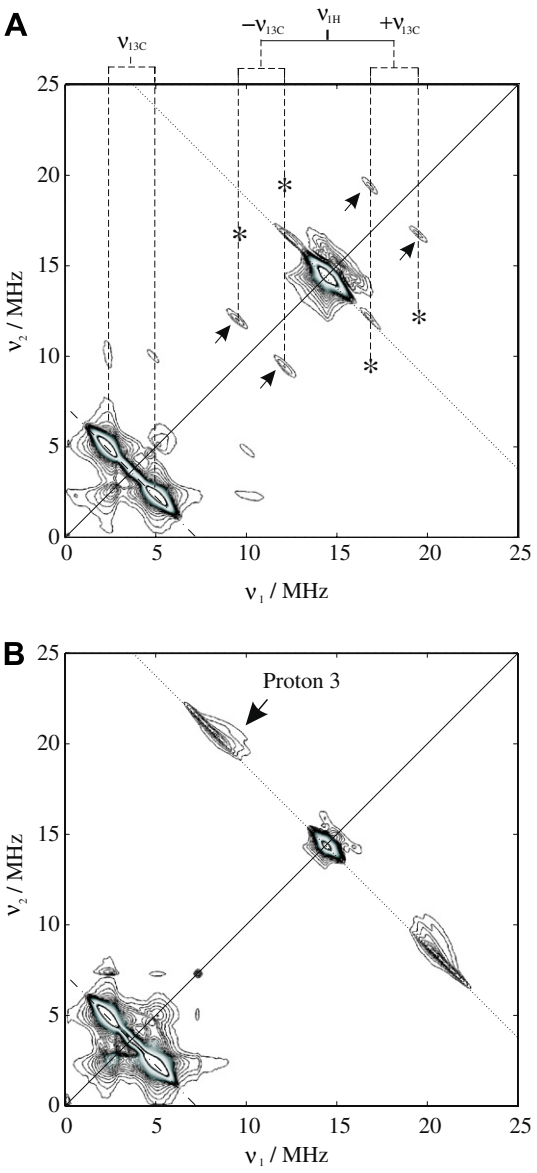

Fig. 8. Comparison between experimental 4-pulse HYSCORE (A) and 6-pulse HYSCORE (B) spectra of ^{63}Cu(Gly-$^{13}C_2$)$_2$ ($B_0 = 3376$ G, $T = 20$ K, $\tau = \tau_2 = 144$ ns and $\tau_1 = 56$ ns). 4-pulse HYSCORE contains (^{1}H,^{13}C)-cross combination peaks, whereas 6-pulse HYSCORE does not.

There are no visible MQ/MQ peaks at $(\omega_{\alpha,^1H} \mp \omega_{\alpha,^{13}C}, \omega_{\beta,^1H} \pm \omega_{\beta,^{13}C})$, marked with stars in Fig. 8A. If a suppressor has a large modulation depth parameter k_r, one also has to consider $a_{4p,2}$; then additional cross-suppression peaks occur at these frequencies. Another effect further reduces peaks at $(\omega_{\alpha,^1H} \mp \omega_{\alpha,^{13}C}, \omega_{\beta,^1H} \pm \omega_{\beta,^{13}C})$; a ridge shape parallel to the diagonal results in destructive phase interference between signals from adjacent orientations in disordered system [36].

In the 6-pulse HYSCORE spectrum in Fig. 8B, as predicted by the numerical simulations and expected from theory, the inter-nuclear MQ/MQ peaks are completely absent, rendering a much less crowded spectrum. Most remarkable about the 6-pulse HYSCORE spectrum is that peaks from proton 3 (Ref. [23]) are visible, whereas they do not appear in the 4-pulse HYSCORE spectrum even though $b^{p3}_{5p} < b^{p3}_{4p}$. Upon closer inspection, it is found that the peak amplitude of proton 3 is increased by a factor of 6 compared to 4-pulse HYSCORE, where the peaks have half the intensity of the ^{1}H-^{13}C MQ/MQ peak and are barely recognizable above the noise level. The splitting of approximately 5 MHz is assigned to originate from proton 1 and is just above the noise level in 6-pulse HYSCORE due to blind-spots $b^{p1}_{5p} \ll b^{p1}_{4p}$.

This power of 6-pulse HYSCORE to reveal nuclei which remain undetected in 4-pulse HYSCORE has already been used in our laboratory in several systems, which will be described elsewhere.

6. Conclusions

Analytical expressions, including product rules, for 5-pulse ESEEM and 6-pulse HYSCORE signals were derived for spin systems containing one unpaired electron coupled to one or more nuclear spins and compared to 3-pulse ESEEM and standard 4-pulse HYSCORE, respectively.

For a single-nucleus spin system, spectral peak intensities consist of two parts: a τ-dependent suppression term and a term depending on the mixing of the nuclear states in the α and β manifolds. For $\tau_1 = \tau_2$, the blind-spot behavior of 5-pulse ESEEM and 6-pulse HYSCORE is similar to an amplified 3-pulse ESEEM and 4-pulse HYSCORE blind spot behavior. It is usually sufficient to acquire 5-pulse ESEEM and 6-pulse HYSCORE data with $\tau_1 = \tau_2$.

The amplitude dependence on the modulation depth parameter k and on the angle η in the various sequences was studied. An SQ peak of a weakly modulating nucleus ($k \approx 0$) is determined by a single amplitude term, which is about eight times larger in 5-pulse ESEEM and 6-pulse HYSCORE compared to 3-pulse ESEEM and 4-pulse HYSCORE. For a nucleus in the intermediate coupling regime ($k \approx 1$), additional terms with different phase contribute to the amplitude, so that the modulation enhancement is less than eightfold.

Compared to a single-nucleus spin system, SQ peak amplitudes in a multi-nuclear spin system are reduced due to the cross-suppression effect. This reduction of the single-quantum peak intensities of weakly modulating nuclei in the presence of strongly modulating nuclei is less severe in 5-pulse ESEEM and 6-pulse HYSCORE compared to 3-pulse ESEEM and 4-pulse HYSCORE, which is mainly due to the enhanced sensitivity towards $k \approx 0$ nuclei. In addition, peaks at inter-nuclear combination frequencies are created in 3-pulse ESEEM and 4-pulse HYSCORE, but are found to be absent in 5-pulse ESEEM and 6-pulse HYSCORE.

Acknowledgment

The authors thank Dr. C. Calle and Prof. G. Jeschke for helpful discussions. The late Prof. A. Schweiger provided

the original idea of examining the utility of 5-pulse ESEEM in reducing the impact of the cross-suppression effect. This research has been supported by the Swiss National Science Foundation.

Appendix A. Phase cycles in 5-pulse ESEEM and 6-pulse HYSCORE

As all multi-pulse sequences, 5-pulse ESEEM and 6-pulse HYSCORE give rise to a number of unwanted echoes that occur at the position of the echo of interest for certain or all values of the incremented time intervals. The phase cycles [17] given in Table 1 can be used to suppress them. In designing these phase cycles, we have neglected free induction decays, since they usually decay within the dead time and do not interfere with the detection of the echo of interest.

The 2-step phase cycle for 5-pulse ESEEM in Table 1(a) was first given in [6]. It removes all unwanted crossing echoes, but retains several 3-pulse echoes that coincide with the 5-pulse echo in the cases $\tau_1 = \tau_2$, $2\tau_1 = \tau_2$, or $\tau_1 = 2\tau_2$. However, due to the pulse flip angles employed, the amplitudes of these echoes (e.g. from $(+,+,0,-,-)$ for $\tau_1 = \tau_2$) are usually small, so that they can be neglected. The 2-step phase cycle also does not remove the 2-pulse echo from the pathway $(0,0,0,+,-)$, which, however, does usually not disturb, as its phase is orthogonal to the 5-pulse echo. A more robust 4-step phase cycle for arbitrary τ_1 and τ_2 is given in Table 1(b).

The original 6-pulse HYSCORE phase cycle proposed in Ref. [7] keeps several unwanted 2- and 3-pulse echoes and is therefore somehow limited to $\tau_1 < \tau_2, \tau_1 \neq \frac{\tau_2}{2}$. Table 1(c) and (d) contain new 6-pulse HYSCORE phase cycle schemes. They are obtained from Table 1(a) and (b), respectively, by cycling the π mixing pulse. The 4-step phase cycle removes all crossing echoes, but retains the out-of-phase two-pulse echo from the last two pulses and several 3-pulse echoes with small transfer amplitudes. The more robust 8-step phase cycle removes the out-of-phase two-pulse echo and most 3-pulse echoes.

For remote echo detected [25] 5-pulse ESEEM and 6-pulse HYSCORE, where the sequence $(\pi/2)_{+y} - T_r - (\pi/2)_{+y} - \tau_r - (\pi)_{+y} - \tau_r - \text{echo}_x$ is added at the point of the echo, no additional phase cycles are needed. The ones in Table 1 can be used, provided that T_r is much longer than the transverse relaxation time T_2.

Appendix B. Simplification of the 5-pulse ESEEM modulation formula ($k_q \ll 1$ for all nuclei q)

In this section we assume that the modulations of the N_I nuclei are either in the weak or strong coupling limit, i.e. $k_q \ll 1$ for all nuclei q. It will be shown that the 5-pulse ESEEM spectrum of a multi-nuclear spin system corresponds to the superposition of the single-nucleus 5-pulse ESEEM spectra.

The first term of the modulation expression of 5-pulse ESEEM (Eq. (20)) is given by

$$E_{2p,q}(\tau_1)E_{2p,q}(\tau_2) = 1 + \mathcal{O}_{2p}(k_q) + \mathcal{O}_{2p}(k_q^2) \overset{k\ll 1}{\approx} 1 + \mathcal{O}_{2p}(k_q), \tag{36}$$

where $\mathcal{O}_{2p}(k_q^2)$ comprises negligible terms proportional to the 2nd power of k_q, and

$$\begin{aligned}\mathcal{O}_{2p}(k_q) = {} & \frac{k_q}{2}\left[-1 + \cos(\tau_1\omega_{\alpha,q}) + \cos(\tau_1\omega_{\beta,q}) - \frac{1}{2}\cos(\tau_1\omega_{-,q}) - \frac{1}{2}\cos(\tau_1\omega_{+,q})\right] \\ & + \frac{k_q}{2}\left[-1 + \cos(\tau_2\omega_{\alpha,q}) + \cos(\tau_2\omega_{\beta,q}) - \frac{1}{2}\cos(\tau_2\omega_{-,q}) - \frac{1}{2}\cos(\tau_2\omega_{+,q})\right].\end{aligned} \tag{37}$$

Table 1
Phase cycles for 5-pulse ESEEM and 6-pulse HYSCORE

	$\pi/2$	π	$\pi/2$	$\pi/2$	π	Det.
(a)	$+y$	$+y$	$+x$	$+x$	$+x$	$+x$
	$-y$	$-y$	$-x$	+x	+x	+x
(b)	$+y$	$+y$	$+x$	$+x$	$+x$	$+x$
	$-y$	$-y$	$-x$	$+x$	$+x$	$+x$
	$+y$	$-y$	$-x$	$-x$	$+x$	$+x$
	$-y$	$+y$	$+x$	$-x$	$+x$	$+x$

	$\pi/2$	π	$\pi/2$	π	$\pi/2$	π	Det.
(c)	$+y$	$+y$	$+x$	$+x$	$+x$	$+x$	$+x$
	$+y$	$+y$	$+x$	$-x$	$+x$	$+x$	$+x$
	$-y$	$-y$	$-x$	$+x$	$+x$	$+x$	$+x$
	$-y$	$-y$	$-x$	$-x$	$+x$	$+x$	+x
(d)	$+y$	$+y$	$+x$	$+x$	$+x$	$+x$	$+x$
	$+y$	$+y$	$+x$	$-x$	$+x$	$+x$	$+x$
	$-y$	$-y$	$-x$	$+x$	$+x$	$+x$	$+x$
	$-y$	$-y$	$-x$	$-x$	$+x$	$+x$	$+x$
	$+y$	$-y$	$-x$	$+x$	$-x$	$+x$	$+x$
	$+y$	$-y$	$-x$	$-x$	$-x$	$+x$	$+x$
	$-y$	$+y$	$+x$	$+x$	$-x$	$+x$	$+x$
	$-y$	$+y$	$+x$	$-x$	$-x$	$+x$	$+x$

(a, b) 5-pulse ESEEM. (c, d) 6-pulse HYSCORE.

The remaining terms

$$\begin{aligned}\mathcal{O}^{\alpha}_{5p}(k_q) = b_{5p,q}k_q[&-4k_qC_0^{\alpha,q}\\ &+4\cos^4\eta_q\cos(T\omega_{\alpha,q}+\phi_{\alpha_{+,q}}+\phi_{\beta_{+,q}})\\ &+2k_q\cos\phi_{\beta_{-,q}}\cos(T\omega_{\alpha,q}+\phi_{\alpha_{+,q}})\\ &+4\sin^4\eta_q\cos(T\omega_{\alpha,q}+\phi_{\alpha_{+,q}}-\phi_{\beta_{+,q}})]\end{aligned} \tag{38}$$

reduce to a single term; in the weak and the strong coupling limit to

$$\mathcal{O}^{\alpha}_{5p}(k_q) \approx 4b_{5p,q}k_q\cos^4\eta_q\cos(T\omega_{\alpha,q}+\phi_{\alpha_{+,q}}+\phi_{\beta_{+,q}}) \tag{39}$$

and

$$\mathcal{O}^{\alpha}_{5p}(k_q) \approx 4b_{5p,q}k_q\sin^4\eta_q\cos(T\omega_{\alpha,q}+\phi_{\alpha_{+,q}}-\phi_{\beta_{+,q}}), \tag{40}$$

respectively. For simplicity, we assume here that all nuclei are weakly coupled (keeping in mind that strongly coupled nuclei are described by a single term). By combining Eqs. (36) and (39), we obtain an approximate expression for the modulation formulas of the α_+ and α_- eCTPs:

$$E^{\alpha_\pm}_{5p,q} \overset{k\ll 1}{\approx} 1+\mathcal{O}_{2p}(k_q)\mp\mathcal{O}^{\alpha}_{5p}(k_q). \tag{41}$$

The signal of the multi-nuclear spin system consist of a product of the single-nucleus modulations (Eq. (23)), which further simplifies according to

$$\begin{aligned}\prod_{q=1}^{N_I}E^{\alpha_\pm}_{5p,q} &= \prod_{q=1}^{N_I}1+\mathcal{O}_{2p}(k_q)\mp\mathcal{O}^{\alpha}_{5p}(k_q)\\ &\overset{k\ll 1}{\approx} 1+\sum_{q}^{N_I}\mathcal{O}_{2p}(k_q)\mp\sum_{q}^{N_I}\mathcal{O}^{\alpha}_{5p}(k_q).\end{aligned} \tag{42}$$

Products of two or more first order terms of k_q are omitted as they result in negligible magnitude, i.e. $\mathcal{O}_{2p}(k_{q1})\mathcal{O}_{2p}(k_{q2})\approx\mathcal{O}_{2p}(k_{q1})\mathcal{O}^{\alpha}_{5p}(k_{q2})\approx\mathcal{O}^{\alpha}_{5p}(k_{q1})\mathcal{O}^{\alpha}_{5p}(k_{q2})\approx 0$.

After summation of the α_+ and α_- pathways,

$$\begin{aligned}E^{\alpha}_{5p} &= \prod_{q=1}^{N_I}E^{\alpha_+}_{5p,q}-\prod_{q=1}^{N_I}E^{\alpha_-}_{5p,q}\overset{k\ll 1}{\approx}-2\sum_{q}^{N_I}\mathcal{O}^{\alpha}_{5p}(k_q)\\ &= \sum_{q}^{N_I}-8b_{5p,q}k_q\cos^4\eta_q\cos(T\omega_{\alpha,q}+\phi_{\alpha_{+,q}}+\phi_{\beta_{+,q}}),\end{aligned} \tag{43}$$

we find that the α SQ peaks of nuclei $q=1,\ldots,N_I$ are described by single terms.

This result is also valid for the β_+ and β_- pathways (exchange α and β in Eqs. (38)–(43)).

Appendix C. 4- and 6-pulse HYSCORE expressions

We use absolute valued nuclear frequencies (Eq. (4)) in the HYSCORE formulas, in order to simplify the illustration of the discussed features. In an alternative convention, *signed* nuclear frequencies together with a different definition of the angle $\eta_{\alpha,\beta}$ [1,13], yield equivalent results. The conclusions developed in this work are independent of the convention employed.

The modulation formula for 4-pulse HYSCORE [1,17,21] following the eCTP $(+,0_\alpha,0_\beta,-)$ is given by

$$\begin{aligned}E^{\alpha\beta}_{4p}(T_1,T_2,\tau) = 1-\frac{k}{2}\Bigg[&\frac{C_0}{2}+C_\alpha\cos\left(\omega_\alpha\left(T_1+\frac{\tau}{2}\right)\right)\\ &+C_\beta\cos\left(\omega_\beta\left(T_2+\frac{\tau}{2}\right)\right)\\ &-2b_{4p}\Bigg(\cos^2\eta\cos\left(\omega_\alpha T_1+\omega_\beta T_2+\omega_+\frac{\tau}{2}\right)\\ &-\sin^2\eta\cos\left(\omega_\alpha T_1-\omega_\beta T_2+\omega_-\frac{\tau}{2}\right)\Bigg)\Bigg]\end{aligned} \tag{44}$$

with

$$\begin{aligned}C_0 = 3&-\cos(\omega_\alpha\tau)-\cos(\omega_\beta\tau)\\ &-\sin^2\eta\cos(\omega_+\tau)-\cos^2\eta\cos(\omega_-\tau),\end{aligned} \tag{45}$$

$$\begin{aligned}C_\alpha = &\cos^2\eta\cos\left(\left(\omega_\beta-\frac{\omega_\alpha}{2}\right)\tau\right)\\ &+\sin^2\eta\cos\left(\left(\omega_\beta+\frac{\omega_\alpha}{2}\right)\tau\right)-\cos\left(\frac{\omega_\alpha}{2}\tau\right),\end{aligned} \tag{46}$$

$$\begin{aligned}C_\beta = &\cos^2\eta\cos\left(\left(\omega_\alpha-\frac{\omega_\beta}{2}\right)\tau\right)\\ &+\sin^2\eta\cos\left(\left(\omega_\alpha+\frac{\omega_\beta}{2}\right)\tau\right)-\cos\left(\frac{\omega_\beta}{2}\tau\right).\end{aligned} \tag{47}$$

and the blind-spot term

$$b_{4p} = \sin(\omega_\alpha\tau/2)\sin(\omega_\beta\tau/2). \tag{48}$$

The modulation along the other pathway, $E^{\beta\alpha}_{4p}$, is obtained by exchanging α and β in the above expressions. The product rule for the unnormalized signal is

$$E_{4p}(T_1,T_2;\tau) = \prod_{q=1}^{N_I}E^{\alpha\beta}_{4p,q}+\prod_{q=1}^{N_I}E^{\beta\alpha}_{4p,q}. \tag{49}$$

In 6-pulse HYSCORE, the modulations for the eCTPs $(\pm,\mp,0_\alpha,0_\beta,+,-)$ are

$$\begin{aligned}E^{\alpha\beta_\pm}_{6p} = E_{2p}(\tau_1)E_{2p}(\tau_2)\mp kb_{5p}[&4k\cos 2\eta C_0\\ &+4\cos^6\eta\cos(T_1\omega_\alpha+T_2\omega_\beta+\phi_{\alpha+}+\phi_{\beta+})\\ &+4\sin^6\eta\cos(T_1\omega_\alpha-T_2\omega_\beta+\phi_{\alpha+}-\phi_{\beta+})\\ &+k\cos^2\eta(C_C+\cos(T_1\omega_\alpha+T_2\omega_\beta+\phi_{\alpha+}-\phi_{\beta-})\\ &+\cos(T_1\omega_\alpha+T_2\omega_\beta+\phi_{\alpha-}+\phi_{\beta+})\\ &+\cos(T_1\omega_\alpha-T_2\omega_\beta+\phi_{\alpha-}+\phi_{\beta-}))\\ &+k\sin^2\eta(C_S+\cos(T_1\omega_\alpha-T_2\omega_\beta+\phi_{\alpha+}+\phi_{\beta-})\\ &+\cos(T_1\omega_\alpha-T_2\omega_\beta+\phi_{\alpha-}-\phi_{\beta+})\\ &+\cos(T_1\omega_\alpha+T_2\omega_\beta+\phi_{\alpha-}-\phi_{\beta-}))]\end{aligned} \tag{50}$$

with the phases $\phi_{\alpha\pm}=(\tau_1\pm\tau_2)\omega_\alpha/2$ and $\phi_{\beta\pm}=(\tau_1\pm\tau_2)\omega_\beta/2$, the abbreviations

$$C_0=\cos\left(\frac{\tau_1\omega_\alpha}{2}\right)\cos\left(\frac{\tau_2\omega_\beta}{2}\right)\sin\left(\frac{\tau_2\omega_\alpha}{2}\right)\sin\left(\frac{\tau_1\omega_\beta}{2}\right), \tag{51}$$

$$\begin{aligned}C_{\mathrm{C}}=&\cos(T_1\omega_\alpha+\phi_{\alpha+}+\phi_{\beta-})-\cos(T_1\omega_\alpha+\phi_{\alpha-}+\phi_{\beta-})\\&+\cos(T_1\omega_\alpha+\phi_{\alpha+}+\phi_{\beta+})-\cos(T_1\omega_\alpha+\phi_{\alpha-}+\phi_{\beta+})\\&+\cos(T_2\omega_\beta-\phi_{\alpha-}+\phi_{\beta+})-\cos(T_2\omega_\beta-\phi_{\alpha-}-\phi_{\beta-})\\&+\cos(T_2\omega_\beta+\phi_{\alpha+}+\phi_{\beta+})-\cos(T_2\omega_\beta+\phi_{\alpha+}-\phi_{\beta-}),\end{aligned} \tag{52}$$

$$\begin{aligned}C_{\mathrm{S}}=&\cos(T_1\omega_\alpha+\phi_{\alpha+}-\phi_{\beta-})-\cos(T_1\omega_\alpha+\phi_{\alpha-}-\phi_{\beta-})\\&+\cos(T_1\omega_\alpha+\phi_{\alpha+}-\phi_{\beta+})-\cos(T_1\omega_\alpha+\phi_{\alpha-}-\phi_{\beta+})\\&+\cos(T_2\omega_\beta-\phi_{\alpha+}+\phi_{\beta+})-\cos(T_2\omega_\beta-\phi_{\alpha+}-\phi_{\beta-})\\&+\cos(T_2\omega_\beta+\phi_{\alpha-}+\phi_{\beta+})-\cos(T_2\omega_\beta+\phi_{\alpha-}-\phi_{\beta-})\end{aligned} \tag{53}$$

and the blind-spot term $b_{5\mathrm{p}}$ from Eq. (21). The modulations for the eCTPs $(\pm,\mp,0_\beta,0_\alpha,+,-)$, $E_{6\mathrm{p}}^{\beta\alpha_+}$ and $E_{6\mathrm{p}}^{\beta\alpha_-}$, are obtained by exchanging α and β in Eqs. (50)–(53). The total unnormalized signal, for any number of nuclei, is

$$\begin{aligned}E_{6\mathrm{p}}(T_1,T_2;\tau_1,\tau_2)=&\prod_{q=1}^{N_I}E_{6\mathrm{p},q}^{\alpha\beta_+}-\prod_{q=1}^{N_I}E_{6\mathrm{p},q}^{\alpha\beta_-}\\&+\prod_{q=1}^{N_I}E_{6\mathrm{p},q}^{\beta\alpha_+}-\prod_{q=1}^{N_I}E_{6\mathrm{p},q}^{\beta\alpha_-}.\end{aligned} \tag{54}$$

References

[1] A. Schweiger, G. Jeschke, Principles of Pulse Electron Paramagnetic Resonance, Oxford University Press, 2001.

[2] Y. Deligiannakis, M. Louloudi, N. Hadjiliadis, Electron spin echo envelope modulation (ESEEM) spectroscopy as a tool to investigate the coordination environment of metal centers, Coord. Chem. Rev. 204 (2000) 1–112.

[3] T. Prisner, M. Rohrer, F. MacMillan, Pulsed EPR spectroscopy: biological applications, Annu. Rev. Phys. Chem. 52 (2001) 279–313.

[4] S. Stoll, C. Calle, G. Mitrikas, A. Schweiger, Peak suppression in ESEEM spectra of multinuclear spin systems, J. Magn. Reson. 177 (2005) 93–101.

[5] C.J. Calle y Richter, Continuous wave and pulse EPR investigations of novel copper(II) and cobalt(II) containing complexes, ETH Diss. 16883, 2006.

[6] C. Gemperle, A. Schweiger, R.R. Ernst, Electron-spin–echo envelope modulation with improved modulation depth, Chem. Phys. Lett. 178 (5,6) (1991) 565–572.

[7] R. Song, Y.C. Zhong, C.J. Noble, J.R. Pilbrow, D.R. Hutton, A new six-pulse two-dimensional electron spin echo envelope modulation (ESEEM) correlation spectroscopy, Chem. Phys. Lett. 237 (1995) 86–90.

[8] W.B. Mims, Envelope modulation in spin–echo experiments, Phys. Rev. B 5 (7) (1972) 2409–2419.

[9] P. Höfer, A. Grupp, H. Nebenführ, M. Mehring, Hyperfine sublevel correlation (HYSCORE) spectroscopy: A 2D ESR investigation of the squaric acid radical, Chem. Phys. Lett. 132 (3) (1986) 279–282.

[10] W.B. Mims, Amplitudes of superhyperfine frequencies displayed in the electron-spin–echo envelope, Phys. Rev. B 6 (9) (1972) 3543–3545.

[11] P. Höfer, Distortion-free electron-spin–echo envelope-modulation spectra of disordered solids obtained from two- and three-dimensional HYSCORE experiments, J. Magn. Reson. A 111 (1994) 77–86.

[12] A. Schweiger, F. Graf, G. Rist, H.H. Günthard, Theory and applications of generalized operator transforms for diagonalization of spin hamiltonians, Chem. Phys. 17 (1976) 155–185.

[13] G. Jeschke, New concepts in solid-state pulse electron spin resonance, ETH Diss. 11873, 1996.

[14] I.S. Podkorytov, Multipulse NMR. Part I. The simplest case: Quantum mechanical treatment of a single-spin system, Concepts Magn. Reson. 8 (1) (1996) 17–32.

[15] I.S. Podkorytov, Multipulse NMR. Part II. Product operator description of the weakly coupled, two-spin-$\frac{1}{2}$ system, Concepts Magn. Reson. 9 (3) (1997) 117–137.

[16] J.J. Shane, Electron spin echo envelope modulation spectroscopy of disordered solids: an investigation of ^{14}N coordination in transition metal complexes, Enschede FEBOdruk, 1993.

[17] C. Gemperle, G. Aebli, A. Schweiger, R.R. Ernst, Phase cycling in pulse EPR, J. Magn. Reson. 88 (1990) 241–256.

[18] A. Ponti, A. Schweiger, Nuclear coherence-transfer echoes in pulsed EPR, J. Chem. Phys. 102 (13) (1995) 5207–5219.

[19] G. Bodenhausen, H. Kogler, R.R. Ernst, Selection of coherence-transfer pathways in NMR pulse experiments, J. Magn. Reson 58 (1984) 370–388.

[20] S.A. Dikanov, A.A. Shubin, V.N. Parmon, Modulation effects in the electron spin echo resulting from hyperfine interaction with a nucleus of an arbitrary spin, J. Magn. Reson. 42 (1981) 474–487.

[21] A.M. Tyryshkin, S.A. Dikanov, D. Goldfarb, Sum combination harmonics in four-pulse ESEEM spectra. Study of the ligand geometry in aqua-vanadyl complexes in polycrystalline and glass matrices, J. Magn. Reson. A 105 (1993) 271–283.

[22] W. Windsch, M. Welter, EPR-Untersuchungen an kupfer-dotierten Triglyzinsulfat- und Glyzin-Einkristallen, Z. Naturforsch. A: Phys. Sci. 22 (1967) 1–8.

[23] M. Fujimoto, C.A. McDowell, T. Takui, Ligand ENDOR spectra of Cu(II) impurity complexes in α-glycine crystals, J. Chem. Phys. 70 (8) (1979) 3694–3701.

[24] L.G. Rowan, E.L. Hahn, W.B. Mims, Electron-spin–echo envelope modulation, Phys. Rev. A 137 (1) (1965) A61–A71.

[25] H. Cho, S. Pfenninger, C. Gemperle, A. Schweiger, R.R. Ernst, Zero deadtime pulsed ESR by remote echo detection, Chem. Phys. Lett. 160 (4) (1989) 391–395.

[26] C. Gemperle, Neue Elektronenspinecho-Experimente, ETH Diss. 9192, 1990.

[27] A. Pöppl, J. Simon, G. Völkel, ^{1}H one- and two-dimensional five-pulse ESEEM investigations on a radiation center in betaine phosphite single crystals, Appl. Magn. Reson. 6 (1994) 455–469.

[28] G. Jeschke, R. Rakhmatullin, A. Schweiger, Sensitivity enhancement by matched microwave pulses in one- and two-dimensional electron spin echo envelope modulation spectroscopy, J. Magn. Reson. 131 (1998) 261–271.

[29] L. Liesum, A. Schweiger, Multiple quantum coherence in HYSCORE spectra, J. Chem. Phys 114 (21) (2001) 9478–9488.

[30] H.L. Flanagan, D.J. Singel, Analysis of ^{14}N ESEEM patterns of randomly oriented solids, J. Chem. Phys. 87 (10) (1987) 5606–5616.

[31] G. Jeschke, A. Schweiger, Matched two-pulse electron spin echo envelope modulation spectroscopy, J. Chem. Phys. 106 (6) (1996) 2199–2211.

[32] R. Szosenfogel, D. Goldfarb, Simulations of HYSCORE spectra obtained with ideal and non-ideal pulses, Mol. Phys. 95 (1998) 1295–1308.

[33] A.V. Astashkin, S.A. Dikanov, V.V. Kurshev, Y.D. Tsvetkov, Dependence of electron spin–echo modulation amplitude on the microwave field intensity, Chem. Phys. Lett. 136 (3,4) (1987) 335–341.

[34] R. Song, Y.C. Zhong, C.J. Noble, J.R. Pilbrow, D.R. Hutton, A new one-dimensional correlation spectroscopy (1D COSY) for electron

spin echo envelope modulation studies, Chem. Phys. Lett. 247 (1995) 477–483.

[35] S.A. Dikanov, M.K. Bowman, Cross-peak lineshape of two-dimensional ESEEM spectra in disordered $S = 1/2$, $I = 1/2$ spin systems, J. Magn. Reson. A 116 (1995) 125–128.

[36] S.A. Dikanov, A.M. Tyryshkin, M.K. Bowman, Intensity of cross-peaks in HYSCORE spectra of $S = 1/2$, $I = 1/2$ spin systems, J. Magn. Reson. 144 (2000) 228–242.

[37] P. Höfer, Distortion-free electron-spin–echo envelope—modulation spectra of disordered solids obtained from two- and three-dimensional HYSCORE experiments, J. Magn. Reson. A 111 (1994) 77–86.

[38] J. Harmer, S. Van Doorslaer, I. Gromov, A. Schweiger, Corrin nitrogens and remote dimethylbenzimidazole nitrogen interactions in Cob(II)alamin studied with HYSCORE at X- and Q-band, Chem. Phys. Lett. 358 (2002) 8–16.